

## Absolute Measurement of $2S$ Atom Production by Dissociative Excitation of Molecular Deuterium\*

Donald M. Cox<sup>†</sup> and Stephen J. Smith<sup>‡</sup>

*Joint Institute for Laboratory Astrophysics, Boulder, Colorado 80302*

(Received 2 December 1971)

We have measured the cross section for production of metastable ( $2S$ ) atoms by the process of dissociative excitation of molecular deuterium by electron impact. The measurement includes the quantitative evaluation of detection efficiency, density, and geometrical factors necessary to establish an absolute scale on a purely experimental basis. The method depends on the application of an rf field at the Lamb-shift frequency (1059 MHz) to quench the metastables at the point of excitation. The radiation induced by the applied field is isotropic so that the absolute cross section depends on a simple solid-angle correction. The cross sections at 23.8 and 39.1 eV are  $2.97 \times 10^{-18}$  and  $3.40 \times 10^{-18}$  cm<sup>2</sup>, respectively, with a probable error estimated to be  $\pm 14\%$ . The energy dependence of the cross section was also measured from threshold to 500 eV.

### I. INTRODUCTION

In this paper we describe a measurement of the total cross section for production of metastable ( $2S$ ) atoms by the process of dissociative excitation of molecular deuterium by electron impact. The measurement includes the quantitative evaluation of detection efficiency, density, and geometrical factors necessary to establish an absolute scale on a purely experimental basis. Our method depends on application of an rf field at the Lamb-shift frequency of 1059 MHz to quench the metastables at the position of the exciting electron beam. Since the radiation produced by rf quenching of the  $2S$  state is essentially unpolarized and isotropic, the Lyman- $\alpha$  flux in any direction, with a simple solid-angle correction, may be taken as a measure of the total cross section for  $2S$  production. This is the first measurement to yield the total  $2S$  production cross section with an experimentally determined absolute scale.

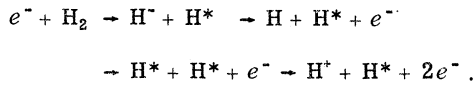
To our knowledge, the first published study of the production of metastable atoms by electron impact on molecular deuterium or hydrogen is that of Lamb and Retherford.<sup>1</sup> They measured the current of electrons ejected from a tungsten surface, on which the metastables were allowed to impinge, as a function of energy of the exciting electrons; however, they did not carry the work beyond a very preliminary observation. Not until the work of Vroom and de Heer<sup>2</sup> was there a deliberate effort to determine the cross section as a function of energy for production of  $2S$  atoms by dissociative excitation of hydrogen and deuterium molecules. Their method was based on the appearance, in a static-gas-filled chamber, of Lyman- $\alpha$  photons associated with the application of an electrostatic quenching field directly to an electron beam, transversely to its axis. The beam was confined by a

longitudinal magnetic field. A normalization was obtained by comparing the production of  $2P$  atoms (obtained with the electrostatic field turned off) to that obtained earlier by Fite and Brackmann<sup>3</sup> in a crossed beam measurement. The latter investigators evaluated their cross section for photon production from molecules by comparing it experimentally with the cross section for production of Lyman- $\alpha$  photons by electron impact on atomic hydrogen, which they had normalized to a Born-approximation calculation.

Fite and Brackmann<sup>3</sup> used an iodine-filled ionization chamber preceded by an oxygen filter, and their comparison of photon count rates obtained with molecular and atomic hydrogen beams yielded a cross section for "countable ultraviolet photons" that is peculiar to their optical system as well as to molecular hydrogen. Vroom and de Heer<sup>2</sup> used a relatively high-resolution spectrograph to isolate the Lyman- $\alpha$  line. Our results are obtained with still a different optical system, a solar blind multiplier preceded by an oxygen filter. We obtain a measurement in zero quenching field that includes Lyman- $\alpha$  photons due to dissociative excitation to the  $2P$  state, and none from the  $2S$  state. However, there is a sizeable component of molecular ultraviolet superposed on the  $2P$  signal. For this reason our results, those of the other workers cited above, and some additional results by McGowan *et al.*<sup>4</sup> cannot be directly compared without explicitly considering the spectral efficiencies of the several systems.

For the  $2S$  signal corresponding to the application of an appropriate quenching field, there is no such ambiguity. Our results are directly comparable to those of Vroom and de Heer<sup>2</sup> and should provide a useful check on the normalization which they obtained indirectly from the Born approximation.

The term dissociative excitation as used here refers to any processes that lead to production of a photon by radiative decay from the  $n=2$  shell of an atom of hydrogen (or deuterium). There are several excitation mechanisms, each with its characteristic threshold; for example,



Our measurement does not distinguish among these several possibilities. Any process leading to the  $2P$  state may be seen as a Lyman- $\alpha$  photon with the quenching field on as well as off. Any process leading to the  $2S$  state may be seen as a Lyman- $\alpha$  photon only when the quenching field is turned on.

The rf-field quenching used in these measurements has a number of important advantages over quenching with electrostatic fields or detection of metastables with a secondary emission detector. The most important advantage has to do with angular anisotropy of products of the electron-impact dissociation process. As pointed out by Dunn,<sup>5</sup> electron-impact dissociation products generally exhibit an angular anisotropy corresponding to a dependence of the excitation probability on the relative orientation of the electron beam and some axis of the original molecule. This anisotropy is typically energy dependent. Electrostatic quenching and secondary emission methods are most conveniently applied at some distance from the exciting electron beam, but for such experimental configurations, the photon flux observed may not be directly proportional to the total cross section. An integration over all angles would be required. Quenching at the excitation site, on the other hand, eliminates the problem of anisotropy of the dissociation products.

Vroom and de Heer<sup>2</sup> applied an electrostatic field at the excitation site to quench the metastables. However, this leads to a compromise between the requirement for adequate quenching efficiency and the requirement that the energy and direction of the electron beam not be unduly disturbed. In fact, it introduces an inconvenient lower limit to the electron energy that can be used. Vroom and de Heer carried out their measurements only above 50 eV. With the rf techniques the threshold for the excitation process is easily accessible. It can be demonstrated that the electron energy and trajectory are affected only negligibly by an rf field of sufficient amplitude for effective quenching.

An additional advantage arises in connection with polarization and angular anisotropy of the Lyman- $\alpha$  flux. Lyman- $\alpha$  radiation from electrostatic quenching of the  $2S$  state of hydrogen has been shown<sup>6,7</sup> to have polarization of approximately

-30% and a corresponding angular anisotropy, because of interference arising from the two transitions  $2^2S_{1/2} \rightarrow 2^2P_{1/2}$  and  $2^2S_{1/2} \rightarrow 2^2P_{3/2}$ . For the rf technique, at 1059 MHz, quenching of the  $2^2S_{1/2}$  state proceeds almost exclusively by transitions to the  $2^2P_{1/2}$  state. It is shown in the Appendix that the polarization for this case is less than 1%.

## II. rf QUENCHING OF H(2S) AND D(2S)

To understand in some detail the effect of an rf field on a hydrogen or deuterium atom in an otherwise field-free region, it is necessary to examine the fine and hyperfine structure<sup>8</sup> of these two atoms. Figure 1 illustrates the hyperfine structure for the  $2^2P_{1/2}$  and  $2^2S_{1/2}$  states of hydrogen and deuterium. The value of the total angular momentum  $F$  for each hyperfine level is also shown. The allowed hyperfine transitions are determined from the selection rules  $\Delta F = 0, \pm 1$ , with  $F=0 \rightarrow F=0$  forbidden. Table I summarizes several important properties of hyperfine transitions between the  $2^2S_{1/2}$  and  $2^2P_{1/2}$  state. The interest is, of course, in those transitions which would lead to depopulation of the  $2^2S_{1/2}$  state. The  $2^2S_{1/2}$  state decays to the ground state with a natural lifetime  $\sim 0.14$  sec, while the radiative lifetime of the  $2^2P_{1/2}$  state is  $1.6 \times 10^{-9}$  sec. The natural level width of the  $2^2P_{1/2}$  state for decay to the ground state is therefore about 100 MHz.

For deuterium, the natural width ( $\sim 100$  MHz) of

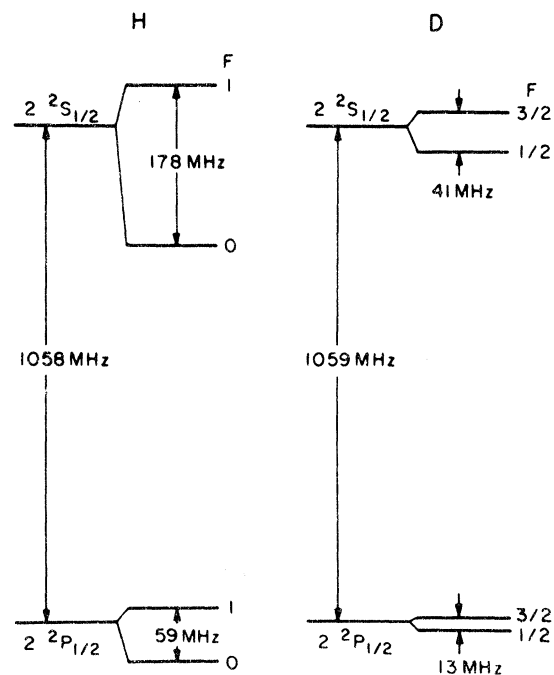


FIG. 1. Hyperfine structure of hydrogen and deuterium for the  $2^2S_{1/2}$  and  $2^2P_{1/2}$  states.

TABLE I. Properties of hyperfine components of the  $2^2S_{1/2} \rightarrow 2^2P_{1/2}$  transitions in atomic hydrogen and deuterium.

Transition	Allowed	Energy	Relative intensity
Hydrogen			
$F=1 \rightarrow F=1$	Yes	1087 MHz	2
$F=0 \rightarrow F=1$	Yes	910 MHz	1
$F=1 \rightarrow F=0$	Yes	1147 MHz	1
$F=0 \rightarrow F=0$	No	969 MHz	0
Deuterium			
$F=\frac{3}{2} \rightarrow F=\frac{3}{2}$	Yes	1068 MHz	10
$F=\frac{1}{2} \rightarrow F=\frac{3}{2}$	Yes	1027 MHz	8
$F=\frac{3}{2} \rightarrow F=\frac{1}{2}$	Yes	1082 MHz	8
$F=\frac{1}{2} \rightarrow F=\frac{1}{2}$	Yes	1041 MHz	1

the  $2^2P_{1/2}$  is greater than the hyperfine splitting of either the  $2^2S_{1/2}$  or  $2^2P_{1/2}$  state (see Fig. 1). In hydrogen the natural width of the  $2^2P_{1/2}$  state is larger than the hyperfine splitting (59 MHz) of the  $2^2P_{1/2}$  state, but is not larger than the hyperfine splitting (178 MHz) of the  $2^2S_{1/2}$  state. Figures 2 and 3 illustrate the hyperfine absorption spectra of hydrogen and deuterium in the frequency range of interest. If a monochromatic rf field at 1060 MHz is used to induce transitions in order to empty the  $F=1$  level, it is well off the center of  $F=0 \rightarrow F=1$  line, the only permitted transition from the  $F=0$  level.

In D(2S), however, all transitions are allowed, but, even more important, the hyperfine splittings are so small that a single radio frequency can be chosen that will be near the centers of all hyperfine lines. Therefore a much lower rf power level can be used to ensure saturation quenching than could be used in the hydrogen case.

In our method an incremental increase in the Lyman- $\alpha$  flux due to the quenching of the D(2S)

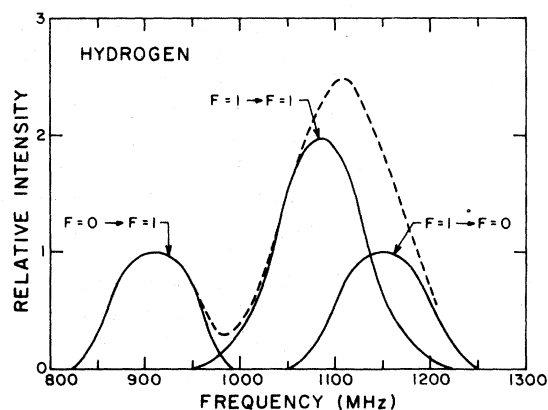


FIG. 2. Relative intensity as a function of frequency for hyperfine transitions in hydrogen ( $2^2S_{1/2} \rightarrow 2^2P_{1/2}$ ).

atom population occurs when an rf field is applied. The amount of the flux increase depends on the intensity of the rf radiation as well as on its frequency, on the speed of the atoms, on their path length in the rf field, and on the metastable production rate. In this measurement the intensity of the rf field was great enough to ensure saturation quenching. That is, metastable atoms produced by the impacting electrons were quenched with very high probability of decaying radiatively to the ground state within the field of view of the Lyman- $\alpha$  detector. The decay rate of the 2S state in an rf field is given by Lamb and Retherford<sup>1</sup> as

$$\frac{1}{\tau_s} = \frac{2\pi e^2 \gamma S_0}{c \hbar^2} \frac{|\langle \hat{e} \cdot \vec{r} \rangle|^2}{(\omega - \omega_0)^2 + (\frac{1}{2}\gamma)^2}, \quad (1)$$

where  $S_0$  is the incident energy flux density of the radiation having circular frequency  $\omega$  and electric polarization parallel to the unit vector  $\hat{e}$ ,  $\omega_0$  is the resonance circular frequency,  $\langle \hat{e} \cdot \vec{r} \rangle$  is the matrix element of the coordinate vector  $\vec{r}$ , and  $\gamma = 1/\tau_p$  is the radiative damping constant for the 2P state. In order to obtain an estimate of  $S_0$  required for a given quenching efficiency, the corresponding lifetime  $\tau_s$  of the 2S state must be determined. This can be found from Eq. (2) which relates the fraction  $\phi$  of atoms quenched by the rf field to the distance  $L$  that the atom travels in the rf field and to the velocity  $v$  of the atoms in field,

$$\phi = 1 - e^{-L/v\tau_s}. \quad (2)$$

By solving Eq. (2) for  $\tau_s$  and substituting into Eq. (1), the required energy flux density  $S_0$  can be found in terms of the fraction  $\phi$  of atoms to be quenched.

### III. APPARATUS

#### A. Configuration

A high-vacuum stainless-steel chamber pre-

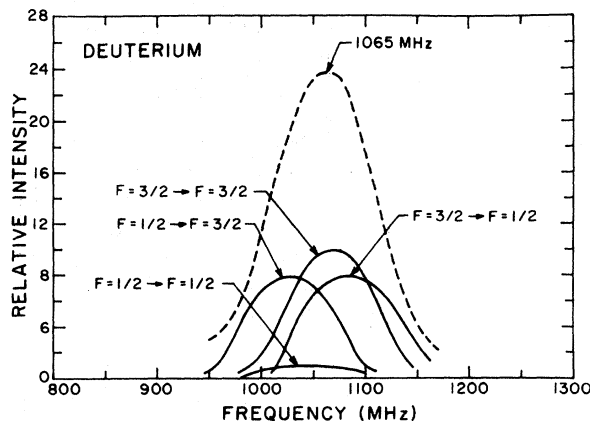


FIG. 3. Relative intensity as a function of frequency for hyperfine transitions in deuterium ( $2^2S_{1/2} \rightarrow 2^2P_{1/2}$ ).

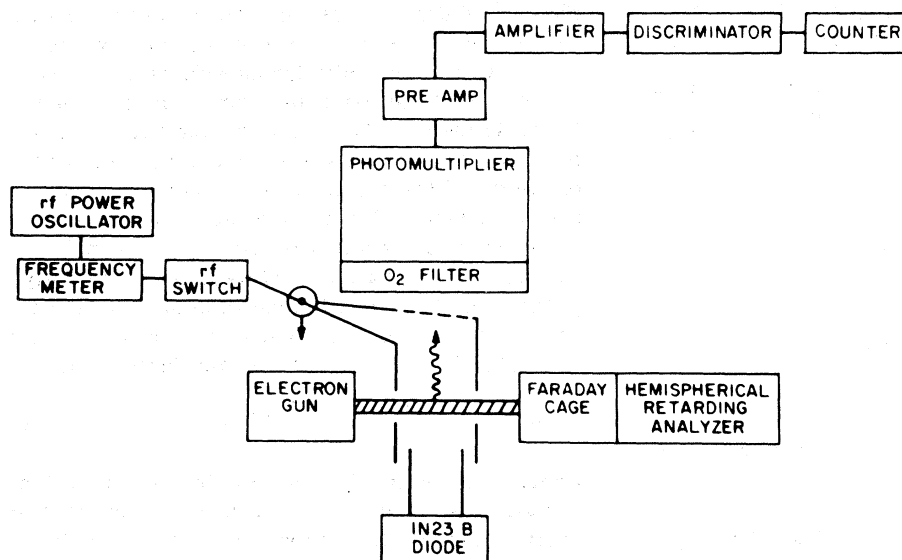


FIG. 4. Simplified block diagram of the experiment.

viously described by Long, Cox, and Smith<sup>9</sup> in connection with crossed beam work was used in this measurement. For our molecular work the beam configuration was unnecessary and the system was used in a static pressure mode. The gas handling system was adapted to allow a slow steady flow of gas through the interaction chamber which was continuously monitored by calibrated ion gauges. A removable stainless-steel ring supported the electron gun and photomultiplier, which were mechanically aligned to each other and to the center of the ring.

A block diagram of the experimental setup is shown in Fig. 4. The electron gun was modified slightly from that described in detail by Long *et al.*<sup>9</sup> A pair of parallel plates installed directly in the interaction region formed the termination of a coaxial line driven by an rf oscillator. As is seen schematically in Fig. 4, the electron beam passed directly through holes in the rf plates. Approximately the same electron energy distribution ( $\sim 0.3$  eV) and contact potential ( $\sim 1.3$  eV) were found as in previous work.<sup>9,10</sup> An additional aperture cut in the upper rf plate allowed the interaction region to be viewed by the photomultiplier that was positioned on an axis perpendicular to the electron beam. Care was taken to minimize stray electric fields by enclosing the interaction region in a grounded cage made of 94% transparent mesh and by shielding electrodes and leads wherever necessary.

#### B. Optics

An EMR 542-J photomultiplier with a semitransparent potassium bromide cathode and a lithium fluoride window was used as the Lyman- $\alpha$  detector. The photomultiplier (unpotted) was operated with

the cathode at negative high voltage allowing the anode to be near ground potential. The multiplier was encased in a metal housing except for the entrance slit, which was covered by a nickel mesh screen. An oxygen filter was attached to the front of the photomultiplier housing. As is well known,<sup>11,12</sup> oxygen strongly attenuates the far-ultraviolet radiation for wavelengths less than 1700 Å, except for several narrow windows, one of which occurs at 1216 Å. At wavelengths greater than 1700 Å, oxygen again transmits, but the photomultiplier response is down by nearly a factor of 300.

The spectral response curve supplied by the manufacturer for this particular photomultiplier is shown in Fig. 5 by the dashed line. The response expected when the oxygen filter was used in conjunction with the photomultiplier is given by the solid line. The narrow windows below the Lyman- $\alpha$  wavelength are not shown, nor is the cutoff (at  $\sim 1100$  Å) due to the MgF windows on the oxygen filter. In the spectral range from 1250 to 1340 Å, oxygen has an important window with an estimated 94% transmission. The filter is also transparent to wavelengths greater than 1700 Å. Since the spectral response of the photomultiplier is quite wide, intense molecular radiation occurring within the window around 1300 Å and at wavelengths greater than 1700 Å would be detected, although at much reduced quantum efficiency. As a result the atomic 2P dissociative excitation signal cannot be completely separated from the molecular radiation allowed by the band pass of the filter-photomultiplier system.

#### C. rf Instrumentation

As shown in Fig. 4, the rf quench field was pro-

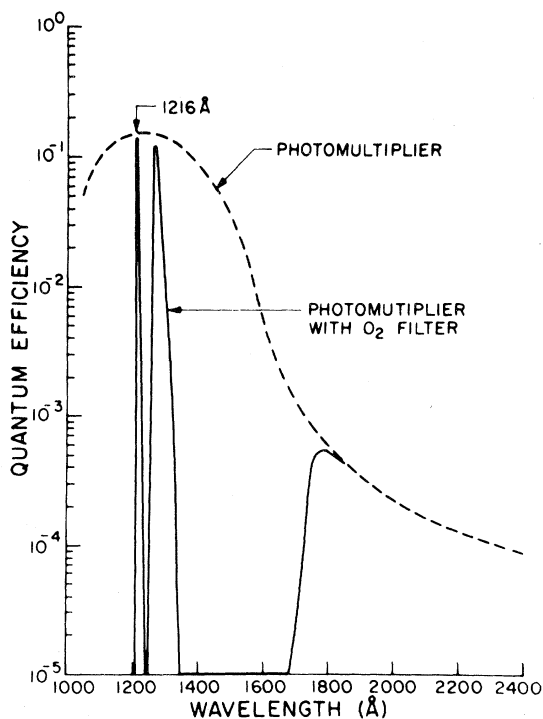


FIG. 5. Photomultiplier response with and without the oxygen filter.

duced by a 10-W power oscillator whose output was regulated by changing the cavity coupling. A frequency meter, tuner (not shown), and a pin diode microwave switch were installed in the output line. The purpose of the frequency meter was twofold. First, it served as a check that the power oscillator was operating in the correct mode at the proper frequency. Second, the frequency meter with its narrow bandpass ( $\sim 2$  MHz full width at half-maximum) would easily be tuned off resonance, thereby cutting off all rf power to the interaction region. The power oscillator itself could be detuned or shut off completely, but this procedure was more time consuming and not as reproducible as detuning the frequency meter. If switched off, even momentarily, the power oscillator tended to drift in frequency and power for several seconds after turn on, before finally stabilizing. The pin diode microwave switch was used to modulate the rf power at the scaler gating frequency and phase. The switch could either pass or block (attenuation approximately 30 dB) the rf power to the interaction region upon application of the proper bias voltage or current to the pin diode switch.

The rf power level in the interaction region was monitored by measuring the voltage developed across an rf diode (IN23B) from which two fine wires extended as antennas into the fringes of the

interaction region. No attempt was made to relate the diode output voltage to the absolute flux at the center of the interaction region; the power level was selected empirically. Figure 6 shows the normalized signal plotted as a function of rf power. The 2S quenching fraction was observed to be  $\frac{2}{3}$  at a diode output voltage of approximately 2 mV. The operating point chosen was in the range 50–150 mV for all measurements. Since the power level is linear with diode output voltage, the fraction quenched at the operating levels is estimated to be greater than 0.999.

The operating-point power levels can be inferred from Eqs. (1) and (2). The distance of travel corresponding to limits of the field of view of the Lyman- $\alpha$  detection system is approximately 0.5 cm. Levanthal *et al.*<sup>13</sup> determined that the velocities of the 2S atoms resulting from the dissociative excitation of deuterium fall into two groups centered at  $2.2 \times 10^6$  and  $6.1 \times 10^5$  cm/sec, the number of atoms produced with the lower velocity being larger than the number produced with higher velocities. Misakian and Zorn<sup>14</sup> obtained velocities agreeing with these within about 50%. The rf power level used to obtain a given quenching fraction can be estimated by using the velocity of the slower group. A range of 140–430 mW/cm<sup>2</sup> is obtained for the operating power level (50–150 mV). Equation (2) indicates that this range provides an adequate safety factor for quenching of the faster 2S atoms.

The effect of the rf field on the electron beam can be estimated from simple dynamical considerations. To minimize the effect of the rf field on the electron trajectories, which are intended to be paraxial, the rf plates are arranged so that the electric field lines are approximately parallel to the electron beam axis. The plane plates are about 1 cm apart, and are perpendicular to the electron beam axis. The electrons pass through holes cut in the plates.

Electron velocities corresponding to the range of energies used in this measurement are  $1.8 \times 10^8$

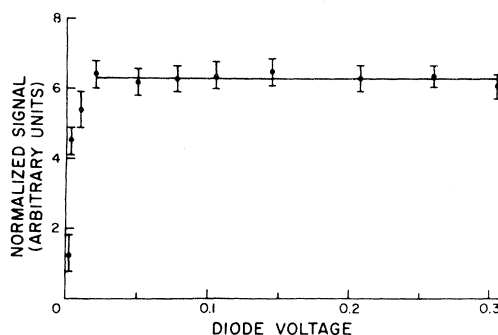


FIG. 6. Quench signal as a function of rf power.

to approximately  $10^9$  cm/sec. The 1059-MHz field then goes through at least one to five full cycles during the passage of an electron through the rf field. The maximum velocity change that electrons can acquire is given by  $eE_m/m\omega$ , where  $E_m$  is the electric field amplitude,  $e$  is the electronic charge,  $m$  its mass, and  $\omega$  the frequency of the applied field. An rf flux density of 500 mW/cm<sup>2</sup> corresponds to a velocity change  $\Delta v = 5 \times 10^6$  cm/sec. For a 10-eV electron this corresponds to a maximum energy shift of 0.007 eV. Since the electron energy is determined to an accuracy of 0.2 eV and the energy spread of the electron beam is typically 0.35 eV in the absence of an rf field, this effect is negligible.

The electron energy spread was examined for a diode voltage of 0.5 V (1400 mW/cm<sup>2</sup>) and the change in the width of the energy distribution, as measured with a retarding spherical analyzer, was less than 0.01 eV.

#### D. Signal Processing and Recording

In this measurement the primary quantity of interest is the difference in photomultiplier signal between the rf field on and off modes. The usual method of data taking was in a pulse counting mode as shown schematically in Fig. 4. The photomultiplier pulses were fed through an inverting preamplifier, main shaping amplifier, and a single channel analyzer before being recorded by a scaler.

The dual-channel scaler was conveniently operated by dc gating as the rf modulation was produced by applying a symmetric square wave to the pin diode microwave switch. Since the response time of the rf switch was only a few nanoseconds and the modulation frequencies were from 100 to 0.05 Hz, the rf power was in correct phase with the applied square wave. A symmetric square wave in phase with the rf modulation square wave was applied to one gate and another square wave 180° out of phase was applied to the other gate, so that one scaler channel recorded the  $2P$  atomic radiation plus the molecular radiation and the other channel measured this same background plus the radiation from the quenching of the metastable atoms in the rf field. To simplify data analysis, care was taken that the square waves applied to the scaler gates were symmetric, which ensured equal duty cycles for each channel.

In general, operating conditions were such that count rates were low. A long counting period was necessary in order to obtain statistically meaningful results. The measurement of the dependence of the 2S dissociative excitation cross section on electron energy required measurements at many electron energies. Because a measurement at each energy generally required counting

times of the order of a few thousand seconds, the data were taken by cycling many times through a preset list of electron energies, with short counting periods of 10–100 sec. This frequent repetition of short observations could thus be used to detect and eliminate the effects of long-term drifts.

It was possible to obtain extremely high count rates ( $10^4$ – $10^5$  counts/sec) by raising the gas pressure and/or electron current. However, at these high count rates pulse pile-up was found to occur in the main amplifier resulting in a nonlinear behavior of the signal as a function of pressure and/or electron current. If, instead of recording pulses the photomultiplier output current was monitored by an electrometer (currents were  $10^{-10}$ – $10^{-7}$  A), the signal was found to exhibit a linear response as a function of pressure at even the highest signal levels.

Because of the slow electrometer response, in this mode the rf field was modulated at 0.05 Hz. One 10-sec integration with the rf field off was completed and recorded, followed by a similar 10-sec integration with the rf field on. Again the difference in these two signals was taken as the metastable signal. The isolation of the pin diode microwave switch could also be checked in this mode of operation. A comparison of the relative 2S signals obtained when modulating the rf power switch with the pin diode switch, to the signals obtained when the rf power oscillator itself was turned on and off, showed the results to be the same. Similarly, simply detuning the frequency meter gave results in agreement with the other two modulation schemes. We conclude that the rf power passed by the pin diode when in the "off" position or by the frequency meter when it was detuned, was negligible.

Modulation at higher frequencies (100 Hz) was also tested using a narrow-band lock-in detector in addition to gated pulse counting. The lock-in scheme could be used at higher count rates than could the pulse-counting system because of pulse pile-up, but still could not be used at the very highest signal levels. The modulated output current from the photomultiplier was applied directly to the input of the lock-in detector. The reference signal for the lock-in was the symmetric square wave used to drive the rf switch. The demodulated output of the lock-in amplifier was then integrated simultaneously with the electron current. In this case the signal is also directly related to the 2S quenching signal, but information about the background signal ( $2P$  plus any molecular radiation) is lost. The lock-in technique was used only for validation of the pulse-counting and dc methods of collecting data.

Because of the enormous amount of data re-

quired during each run (typically 1–3 days were needed to complete a run), automatic data recording was a necessity. A data-acquisition system was employed that periodically and automatically recorded the counts totaled by the two scalers, elapsed time, electron current, cathode potential, gas pressure, 1N23B diode voltage, plus any other relevant parameters. The data were recorded on punched paper tape. The paper tape was then used to generate a magnetic tape from which the data were edited and reduced by a digital computer.

#### IV. ABSOLUTE MEASUREMENT

##### A. Quantitative Basis

The cross section for the production of metastable 2S atoms from dissociative excitation of molecular deuterium by electron impact can be related to the various physical parameters in the following manner. The number  $N$  of metastable atoms produced per second when the electron beam passes through the molecular deuterium gas is directly proportional to the gas density  $n$ , to the electron current  $I_e$ , and to the electron path length  $l$  from which metastable production can be detected. Therefore, we have

$$N = \sigma n l I_e / e, \quad (3)$$

where the constant of proportionality  $\sigma$  is the cross section and  $e$  is the electronic charge. If all the metastable atoms produced could somehow be detected, then Eq. (3) would yield a value for  $\sigma$ , since all other parameters can be measured experimentally.

A practical experimental design is more likely to involve collection of some known fraction of the total number of metastable atoms produced. Methods based on surface detection or on quenching at a distance from the point of production, require that the angular distribution of the dissociation products be known. Dunn<sup>5</sup> has shown that products of dissociation by an electron beam cannot be assumed to have an isotropic angular distribution, so that this distribution must be determined as part of any valid measurement. A principal feature of the work described in this paper is the direct application of an rf quenching field at the excitation site to produce a detectable Lyman- $\alpha$  signal. Since the metastable atoms produced are immediately quenched and since the radiation pattern from metastables quenched at the Lamb-shift frequency is isotropic, the photon signal is related to the metastable production rate through fixed solid angle  $\Omega$  and effective photomultiplier efficiency factor  $Q'$ . Here  $Q' = \tau_0 G Q$ , where  $\tau_0$  is introduced to take account of the transmission of the oxygen filter and three nickel meshes,  $G$  is

the multiplier gain, and  $Q$  is the quantum efficiency of the photocathode. Quantitative evaluation of these factors is adequate for the determination of an absolute metastable production rate  $N$ , from the photon count rate  $C$ :

$$N = 4\pi C / \tau_0 G Q \Omega. \quad (4)$$

The absolute cross section is then expressed as

$$\sigma = \frac{C}{\tau_0 G Q (\Omega/4\pi) (nl) (I_e/e)}. \quad (5)$$

The variable quantities  $I_e$ ,  $C$ , and pressure  $P$  were systematically recorded as part of the lengthy process of accumulating count-rate data. The fixed quantities  $\tau_0$ ,  $\Omega$ , and  $l$  and the product  $G' = GQ$  were determined absolutely in separate calibrations and measurements. Pertinent details of absolute determination of these parameters will be described in the following sections.

##### B. Determination of Gas Density

The density of an ideal gas is given by

$$n = P/kT, \quad (6)$$

where  $n$  is the number of molecules per unit volume,  $k$  is Boltzmann's constant,  $P$  is the measured gas pressure, and  $T$  the absolute temperature. Uncertainty in the density is then primarily due to the uncertainty in the pressure determination plus that due to thermal variations and gradients.

In measurements on the electron-impact excitation of  $N_2$ , Stanton and St. John<sup>15</sup> found about a 19% decrease in their signal from a cool gun to a hot gun. This large decrease corresponds to an interaction-region gas temperature effectively controlled by the gun temperature. The problem can be quite serious if the interaction region is effectively enclosed by electrodes thermally coupled to the gun. Therefore, our experimental design utilized a 94% transparent screen on four sides of a roughly cubic interaction region to couple into the much larger ( $\sim 1$  m<sup>3</sup>) room-temperature volume surrounding it. The mean free path of the molecules is much larger ( $>40$  cm) than the dimensions of the interaction region ( $\sim 1$  cm). The geometry of our system is such that the "hot" electrodes subtend at most 40% of the total solid angle at the center of the interaction region. By actual measurement the gun electrodes nearest the interaction region have a mean equilibrium operating temperature  $\sim 33$  °C higher than that of the larger volume. We estimate that the density is 2% lower in the interaction region than that indicated by the absolute pressure gauge. The cross-section values presented in this paper have been raised by 2% to reflect this correction.

A McLeod gauge<sup>16</sup> connecting directly to the

TABLE II. Pressure-measurement error distribution.

Effect	Uncertainty
(i) Gauge volume and capillary area	$\pm 1\%$
(ii) Capillary depression (Refs. 17-21)	$\pm 3\%$
(iii) Ishii effect (Refs. 21-24)	$\begin{matrix} +2.5\% \\ -0\% \end{matrix}$
(iv) Thermal transpiration due to nonsymmetrical cold trap (Refs. 25-27)	$\begin{matrix} +0\% \\ -2\% \end{matrix}$
(v) Miscellaneous effects (Refs. 29 and 30)	$\pm 1\%$

interaction chamber was used to calibrate two ion gauges. Since a single pressure reading using the McLeod gauge took on the order of 15 min, the outputs of the two calibrated ion gauges were continuously monitored and recorded simultaneously with other measurable parameters, such as the photomultiplier signal, electron current, and electron energy.

Rather intricate factors determine the absolute accuracy of the measurement of pressure with the McLeod gauge, in which gas at the working pressure is compressed by a known volume ratio to a pressure capable of producing a displacement in a manometer. Since density determination is one of the principal sources of systematic error in this absolute measurement, these factors are discussed below. A summary of the major effects leading to an uncertainty in the absolute value of the density is given in Table II. Detailed discussions of the various effects can be found in the references.

The McLeod gauge had a volume of  $2195 \pm 2 \text{ cm}^3$ , with a capillary diameter of  $0.535 \pm 0.001 \text{ mm}$  (values supplied from the manufacturer). Therefore, an uncertainty  $[(\Delta P/P) = (\Delta V/V) + (\Delta A/A)]$  of approximately 1% is built into the system and one cannot expect to do better than 1% on any scale. This value is entered under item i in Table II.

The capillary depression effect is well documented<sup>17-20</sup> but the fact remains that the details of the behavior of any McLeod gauge will depend on the immediate history of the system. This means that the capillary depression effect should be determined at the time of each use. A measurement of the difference in the capillary depression between the open and closed capillary of the McLeod gauge under the condition of a sticking vacuum (less than  $4 \times 10^{-8}$  Torr) over the height of the capillaries gave results reproducible to  $\pm 0.15 \text{ mm}$  with the tapping of both capillaries. This amounts to a pressure uncertainty of  $\pm 3\%$  at  $10^{-5}$  Torr.

The Ishii effect,<sup>21-23</sup> due to the streaming of mercury vapor from the McLeod gauge toward a cold trap, results in pumping of gas out of the McLeod gauge. This effect supposedly can be reduced by introducing a short section of small-bore tubing (2-mm diam  $\times$  2 cm long in this apparatus)

within the main connection between the gauge and the cold trap. Following Ishii and Nakayama<sup>22</sup> we calculated the uncertainty in the pressure to be 0.5% for the present system. However, if Tunnicliff and Rees<sup>24</sup> are correct, the error due to the Ishii effect may be much larger than that estimated above. They point out that a practical system that has been operating for some time without baking may be expected to have a mercury coating on all walls and tubes of the McLeod gauge and as a result may act as a distributed source of mercury vapor. The only important section of tubing might well be that immediately adjacent to the cold trap, not just the smallest diameter section as assumed above. If their suggestion is indeed correct and applicable to every species of gas, the uncertainty in the pressure due to the Ishii effect for the present system becomes  $\begin{matrix} +2.5\% \\ -0\% \end{matrix}$ . This larger estimate will be used until the problem is further clarified; it is entered in item (ii) of Table II. Asymmetrical errors have been assigned indicating that the true pressure is higher than that measured by the McLeod gauge.

Investigations<sup>25-27</sup> have shown that the presence of a nonsymmetrical cold trap between two gauges can introduce a pressure difference between them because the flow, for example, may be viscous in a large diameter section and molecular in a small diameter section. Since different equilibrium conditions exist for viscous and molecular flow across such thermal gradients the trap can support a pressure differential. Following Edmunds and Hobson<sup>27</sup> we have estimated an asymmetrical error of  $\begin{matrix} +0\% \\ -2\% \end{matrix}$  due to this thermal transpiration effect of the cold trap used with this system, which indicates that the true pressure tends to be lower than that measured by the McLeod gauge.

Other effects that may slightly affect the accuracy have been grouped together under item (v) in Table II. These effects include such things as (a) hysteresis, (b) room temperature changes, (c) the electrical charging up of mercury, (d) use of the ideal-gas equation instead of the slightly better van der Waals equation state,<sup>28</sup> (e) slight deviations from Boyle's law, (f) condensible contaminants present in the system,<sup>29</sup> and (g) adsorption and desorption<sup>30</sup> of gas on the walls of the system. The total uncertainty in the pressure measurement is then  $\begin{matrix} +7.5\% \\ -7\% \end{matrix}$ .

The two ion gauges used were a Varian nude millitorr ionization gauge and an ETI 4336 P ionization gauge. The millitorr ionization gauge had previously been commercially calibrated against an elaborate McLeod gauge<sup>31</sup> with hydrogen gas. The calibration *in situ* agreed with the commercial calibration well within the combined uncertainties. The calibrations on the present system were carried out using both hydrogen and deuterium gas ad-

mitted to the system through a silver-palladium leak. No difference in ion gauge or McLeod gauge operation was observed between the two gases.

### C. Radiometry

The absolute value of the product  $G' = GQ$  of the quantum efficiency and the gain of the photomultiplier was measured for Lyman- $\alpha$  photons (1216 Å) by using a vacuum ultraviolet monochromator and a hydrogen discharge lamp. The intensity of the Lyman- $\alpha$  radiation passed by the monochromator was much greater than the most intense molecular radiation passed in the wavelength range of interest 1130–1340 Å. The Lyman- $\alpha$  flux at the monochromator exit was measured by a nitric-oxide-filled ionization chamber with a magnesium fluoride window. Nitric oxide gas was continuously flowed through the cell at a pressure sufficient to ensure absorption of all Lyman- $\alpha$  photons entering the cell. The cell was operated at a voltage insufficient to produce cascading, but sufficient to ensure collection of the total ionization current. Several interchanges of the nitric oxide cell and the photomultiplier were made to obtain statistically meaningful results. Each interchange took several minutes to complete; therefore the instabilities and drift in the hydrogen discharge lamp contributed significant uncertainties to the calibration.

The absolute photon flux  $S_0$  incident upon the nitric oxide cell can be calculated from

$$i_n/e = \tau' S_0 \gamma, \quad (7)$$

where  $i_n$  is the ion current from the nitric oxide cell,  $\tau'$  the transmission of the magnesium fluoride window of the nitric oxide cell, and  $\gamma$  the photoionization efficiency<sup>12</sup> for nitric oxide. The same flux ( $S_0$ ) would be incident upon the photomultiplier if there were no drifts in the source between interchanges. The photomultiplier current  $i_p$  can then be related to the incident flux by

$$i_p/e = S_0 G'. \quad (8)$$

Substitution of Eq. (8) into Eq. (7) yields the simple relation

$$G' = (i_p/i_n)\gamma\tau'. \quad (9)$$

The value of  $G'$  thus measured was  $4.88 \times 10^4 \pm 10\%$  at 3200 V. The value of  $\gamma$  used was 0.81, that reported by Watanabe, Matsunaga, and Sakai.<sup>12</sup> The transmission  $\tau'$  of the nitric oxide cell window was accurately measured to  $\pm 0.3\%$ . The major contribution to the uncertainty in  $G'$  was  $\pm 8\%$  because of instabilities and decay of the absolute photon flux. The value of 0.81 for  $\gamma$  was estimated to be accurate to  $\pm 2\%$ , which contributes the remaining uncertainty.

The oxygen filter positioned directly in front of

the photomultiplier consisted of two 1 mm thick and 1-in. diam magnesium fluoride windows attached to a stainless-steel body and separated by 1.5 mm. Oxygen gas at local atmospheric pressure ( $\sim 620$  mm of Hg) flowed continuously through the cell. The fraction of the Lyman- $\alpha$  radiation transmitted through the oxygen was calculated to be  $0.94 \pm 0.02$ , with the uncertainty primarily due to the value of the oxygen absorption cross section<sup>11</sup> at the Lyman- $\alpha$  wavelength. The transmission of the magnesium fluoride windows was measured to be  $0.607 \pm 0.010$ . The fraction of Lyman- $\alpha$  radiation transmitted by the oxygen filter is then  $0.345 \pm 4\%$ .

The Lyman- $\alpha$  flux was further attenuated by three nickel mesh screens positioned between the photomultiplier and the interaction region. The purpose of the screening was to shield the interaction region from any stray electric fields (e. g., high voltage of the photomultiplier) and also to shield the photomultiplier from the rf field applied in the interaction region. The transmission of each of these screens was measured to be  $0.939 \pm 0.5\%$ . The value of the total transmission  $\tau_0$  in Eq. (5) then becomes  $0.286 \pm 5.5\%$ .

A two-slit system was used to define  $l$  and  $\Omega$ . Following Bederson and Fite<sup>30</sup> one can derive an expression for  $l\Omega$  in terms of known physical dimensions by assuming the electron-beam diameter is small compared to the distance from the center of the interaction region to the defining slit. In the present experiment a maximum uncertainty due to the finite electron beam diameter is estimated to be  $\pm 3\%$  and the error in measurement is  $\pm 1.5\%$  which corresponds to an absolute uncertainty in measurement of  $\pm 0.1$  mm.

### D. Electron Collection

The absolute electron current was determined by collecting the electrons in a Faraday cage and measuring the resulting current with an electrometer. A microampere source (accuracy  $\pm 0.25\%$ ) was used as the primary standard to calibrate the electron current meter.

An uncertainty in the total electron current may result from incomplete collection of all electrons passing through the interaction region. The escape of primary or secondary electrons from the Faraday cage could lead to erroneous values of total electron current, as would the failure of electrons which have passed through the interaction region to enter the Faraday cage. No magnetic field was used to collimate the electron beam. The initial reflection of electrons from the rear of the cage was assumed to be approximately diffuse. The solid angle subtended by the entrance aperture at the rear of the cage was only about 0.01 sr, which ensured a high collection efficiency. This was

checked by applying bias voltages to the Faraday cage. No change in collection efficiency could be observed.

The minimization of the electron current to an annular guard electrode positioned directly in front of the Faraday cage was taken as the condition of optimum focus. The current to this guard ring could always be made less than 0.5% of the total current collected in the Faraday cage. An asymmetrical error for the absolute uncertainty in the electron current was then estimated to be  $\pm 0.25\%$ , with  $\pm 0.25\%$  occurring because of uncertainties in meter calibration and  $\pm 0.0\%$ , and  $-0.5\%$  arising from incomplete collection of all electrons.

#### E. Operational Tests and Errors

The normalized signal (photomultiplier output divided by gas pressure and electron current) was found to be constant to  $\pm 3\%$  from 0.2 to 30  $\mu\text{A}$  of electron beam current. Figure 7 shows a typical electron current linearity check (electron energy 40 eV). This check was obtained, with zero applied quenching fields, by varying the electron current while holding the gas pressure constant. Normal operating currents were between 2 and 10  $\mu\text{A}$  dependent upon the electron energy. The electron current was held constant at each energy, but no attempt was made to equalize the currents at different electron energies. The constancy of the normalized signal over a wide range of electron currents is strong experimental evidence that space-charge quenching of the metastable atoms is a negligible effect. This is consistent with the result of a simple calculation of space-charge fields for the electron currents and geometries used. Maximum space-charge fields are 0.1 or 0.2 V/cm, which corresponds to a lifetime for the 2S atom of about 10 msec or more. A negligible fractional quenching is predicted.

When the pressure was varied from  $3 \times 10^{-6}$  to  $8 \times 10^{-4}$  Torr while holding the electron current constant, the normalized signal was found to be constant as a function of pressure. The atomic deuterium density (arising only from dissociation products) was quite low, which led to the conclusion that imprisonment of resonance radiation is negligible. Similarly the molecular deuterium density (max  $8 \times 10^{-4}$  Torr) is sufficiently low to ensure negligible dissociative excitation of two or more molecules by a single electron. The constancy of the normalized signal as a function of pressure is experimental verification of these conclusions.

If a metastable atom encounters a molecular ion, it may be quenched by the local field of the ion. This effect was discussed by Leventhal *et al.*<sup>13</sup> and was found to be negligible in their experiment for the worst case of complete neutralization of a 0.5-mA primary electron beam. Because the electron

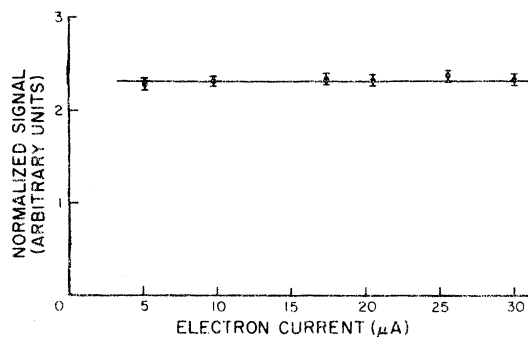


FIG. 7. Quench signal linearity as a function of electron beam current.

currents in the present experiment are on the order of 10  $\mu\text{A}$  maximum, the effect is even less here. Positive ion quenching should be a sensitive function of bombardment current and gas pressure as well as modulation frequency. The linearity of our normalized signal as a function of current and pressure, and the agreement of our results obtained at 100- and at 0.05-Hz modulation frequency indicate that molecular ion quenching is unimportant.

Other effects which must be considered include polarization of the emitted radiation. The polarization has been calculated to be less than 1% for an rf quenching field at 1060 MHz. The Appendix outlines these calculations.

Lyman- $\alpha$  radiation resulting from cascade to the  $n=2$  state from higher-lying states ( $n \geq 3$ ) cannot be differentiated from Lyman- $\alpha$  radiation coming from the direct dissociative excitation to the  $n=2$  level. Vroom and de Heer<sup>2</sup> have shown that most of the Balmer radiation will contribute to the  $2P$  state population with negligible amounts to the 2S state. Excitation to the  $n \geq 4$  states is small compared to the  $n=3$  excitation. Following the arguments of Vroom and de Heer<sup>2</sup> we estimate an upper limit for the cascade cross section at 50 eV of

$$\sigma_{\text{casc}}(1s, 2s) \lesssim 0.035 \times 10^{-18} \text{ cm}^2.$$

At 50 eV this is approximately 1% of the total 2S dissociative excitation cross section with the contribution decreasing at higher electron energies. No correction is applied to our data.

An enhancement of the signal into the photomultiplier from reflections of Lyman- $\alpha$  photons off various surfaces in the interaction region would show up as an erroneously large cross section. From the work of Johnson,<sup>32</sup> in which the hemispherical reflectance of Lyman- $\alpha$  from various surfaces was measured, and from geometrical considerations the signal enhancement due to reflections was estimated to be  $\leq 0.5\%$ .

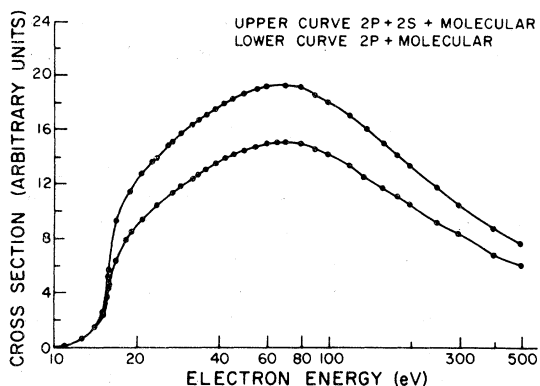


FIG. 8. Energy dependence of the  $2P$ -plus-molecular and  $2P$ -plus- $2S$ -plus-molecular cross sections.

#### F. Absolute Values

An accurate measurement of the absolute cross section was attempted at two different electron energies, 23.8 and 39.1 eV. Since the normalized signal was found to be linear with pressure over all pressures which could be accurately measured with the McLeod gauge, a deuterium gas pressure of approximately  $6 \times 10^{-5}$  Torr was arbitrarily chosen for making the absolute measurement. The absolute values for the cross section determined at the two electron energies are  $2.97 \times 10^{-18}$  and  $3.40 \times 10^{-18}$  cm<sup>2</sup> for 23.8 and 39.1 eV, respectively.

The maximum estimated uncertainty associated with these measurements is  $\pm 28\%$ . This uncertainty is the simple sum of the uncertainties in the several measured experimental quantities. The most probable error, the square root of the sum of the squares of the individual errors, is  $\pm 14\%$ . The use of the most probable error is justified if the individual errors are independent. This is

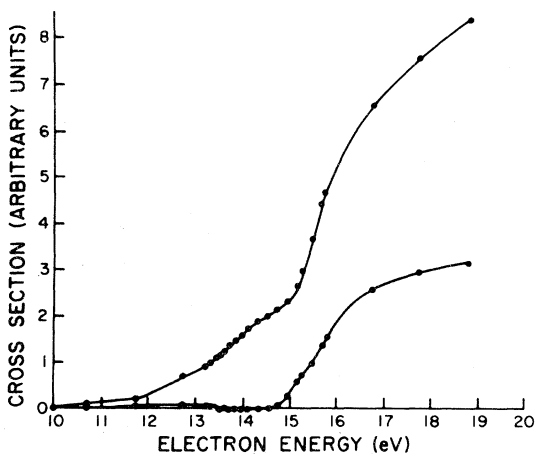


FIG. 9. Threshold behavior of the  $2S$ - and  $2P$ -plus-molecular cross sections.

believed to be the case in these measurements.

## V. RELATIVE CROSS SECTIONS

### A. Search for Structure

The energy dependence of the background ( $2P$  plus molecular radiation) and background plus signal ( $2S$  radiation) is shown in Fig. 8 for the energy range from below threshold to 500 eV. Figure 9 illustrates the threshold behavior of the  $2P$  plus molecular radiation cross section and the  $2S$  dissociative excitation cross section. The relative  $2S$  dissociative excitation cross section over the entire energy range studied is shown in Fig. 10.

As can be seen in Fig. 8, little structure was apparent in the  $2P$  plus molecular excitation cross section. The general shape with a broad maximum between 60 and 80 V agrees reasonably well with that found by McGowan *et al.*<sup>4</sup> The threshold for  $2P$  excitation was assumed to be defined by the large increase in the  $2P$  plus molecular cross section at approximately 14.8 eV. Because the rise was not well defined, the threshold is given as  $14.8 \pm 0.6$  eV. The uncertainty in the threshold is primarily due to the fact that the molecular radiation present tends to wash out any structure and not due to an uncertainty in the electron energy.

The  $2S$  dissociative excitation cross-section threshold, on the other hand, has a fairly well-defined threshold at  $14.8 \pm 0.3$  eV. This is in excellent agreement with the threshold predicted by the sum (14.7 eV) of the excitation energy (10.2 eV) and the dissociation energy (4.5 eV) for the process  $e + D_2 \rightarrow D(2S) + D(1S) + e$ . The uncertainty in the threshold is primarily due to the uncertainty ( $\pm 0.2$  eV) in the determination<sup>11,12</sup> of the electron energy scale. The over-all shape of the  $2S$  cross section as shown in Fig. 10 is thought to be accurate ( $\sim 50\%$  confidence) to  $\pm 2\%$ .

Misakian and Zorn<sup>14</sup> obtained excitation functions for the fast and slow  $H(2S)$  components produced by dissociative excitation of  $H_2$ . Their observa-

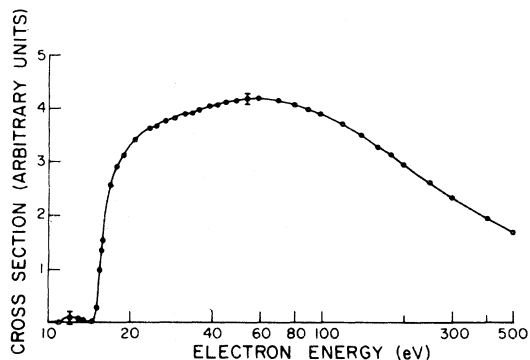


FIG. 10. Energy dependence of the  $2S$  cross section.

tions were at an angle of  $85^\circ$  to the electron beam. Quantitative comparison of their results with the present results on dissociative excitation of  $D_2$  would have to be qualified because of questions of angular distributions and isotope effects. There are qualitative similarities, both rising steeply from threshold to about 20 eV, then rising more slowly to a maximum below 100 eV (taking the composite of Misakian and Zorn's fast and slow excitation functions). However, the amplitude of their function is relatively much smaller at 20 eV than that shown in Fig. 10.

Several energy regions were closely examined for possible structure. A minimum threshold for the process  $e^- + D_2 \rightarrow D^* + D^* + e$  is estimated to be approximately 25 eV if one takes the sum of the excitation energies (20.4 eV) and the dissociation energy (4.5 eV). The minimum threshold for process  $e + D_2 \rightarrow D^+ + D^* + 2e$  is estimated to be approximately 28 eV. No distinct thresholds were observed in this energy range. This is consistent with the work of Misakian and Zorn<sup>14</sup> and also with the work of Leventhal *et al.*<sup>13</sup>

The threshold for molecular radiation appears to be between 11 and 12 eV, which is consistent with the findings of McGowan *et al.*<sup>4</sup> Not observed in the present measurements of  $D(2P)$  plus molecular cross section is a small threshold near 28 eV corresponding to that observed in the  $H(2P)$  dissociative excitation measurements of McGowan *et al.*<sup>4</sup>

The region between 13 and 15 eV was also examined with a fine grid of electrons energies in an attempt to observe Lyman- $\alpha$  radiation from the process  $e^- + D_2 \rightarrow D^* + D^-$ , where the excited atom  $D^*$  is in the  $n = 2$  shell. The total cross section for dissociative attachment in  $H_2$ , HD, and  $D_2$  has been measured by Rapp *et al.*<sup>33</sup> in the energy range 7–18 eV. They found three main peaks, one of which occurred near 14 eV and was interpreted by them as due to an excited  $H_2^-$  state asymptotic to  $H(n = 2) + H^-$ . They found a strong isotope effect. The total dissociative attachment cross section for  $D_2$  was found to be about one-half that for  $H_2$ . The value for the dissociative attachment cross section for  $D_2$  at the 14-eV peak was about  $1 \times 10^{-20} \text{ cm}^2$ . The upper curve in Fig. 9 shows a slight rise between 13 and 15 eV. The value of the  $2P$  plus molecular cross section in our measurements at 14 eV is approximately  $1.2 \times 10^{-18} \text{ cm}^2$ . If the entire  $D^-$  formation in this energy range were accompanied by  $D(2P)$  formation, the result would be approximately a 1% effect on the  $2P$  plus molecular cross section. The observed slight rise is consistent with this description. However, the molecular radiation cross section in this region may be of the order of 1%, so that no quantitative conclusion can be drawn. Any  $2S$  formation should be at least a factor of 2 lower.<sup>2</sup> No indication of Ly-

man- $\alpha$  production could be found in the quenched radiation in the energy range between 13 and 15 eV.

#### B. Comparison with Vroom and de Heer

Vroom and de Heer<sup>2</sup> reported measurements of the dissociative excitation cross section for hydrogen and deuterium between 50 and 6000 eV. In Fig. 11 the present results are shown to fall considerably below the Vroom and de Heer results. Vroom and de Heer<sup>2</sup> have normalized their relative emission cross sections for Lyman- $\alpha$  radiation to the cross section for the production of countable ultraviolet radiation in the case of electrons incident upon molecular hydrogen as measured by Fite and Brackmann.<sup>3</sup>

If one uses a vacuum monochromator for Lyman- $\alpha$  detection, as did Vroom and de Heer,<sup>2</sup> the normalization to the cross section of Fite and Brackmann<sup>3</sup> is valid only if the cross section for production of countable ultraviolet radiation is equal to the cross section for Lyman- $\alpha$  production by electrons on  $H_2$ . The assumption by Vroom and de Heer that this was approximately true has been found to be incorrect. Subsequent measurements by Carrière and de Heer<sup>34</sup> have shown that for electrons incident upon molecular hydrogen a large fraction (approximately 27%) of the radiation passed by an oxygen filter results from molecular radiation. This implies that the Vroom and de Heer results are too high.

Another check was provided by recent measurements by de Heer and Carrière,<sup>35</sup> in which the cross sections for the Werner bands in hydrogen were measured. These cross sections were put on an absolute scale by normalization to theoretical Born or Bethe cross sections, evaluated by means of the theoretical generalized oscillator strengths

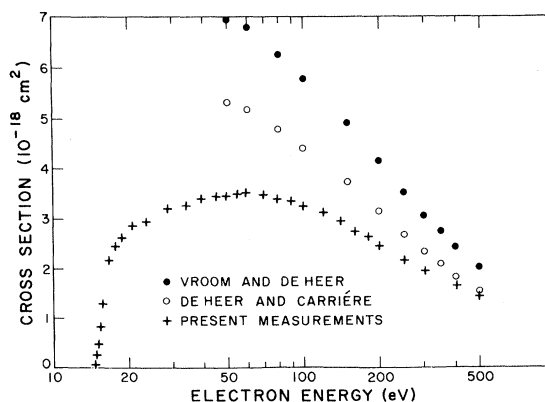


FIG. 11.  $2S$  dissociative excitation cross section. The open circles are the Vroom and de Heer (Ref. 2) results lowered by a factor of 1.31 as determined by de Heer and Carrière, and corrected for polarization.

TABLE III. Measured values of the cross section<sup>a</sup> for dissociative excitation of molecular deuterium with a 2S-state product atom.

Electron <sup>b</sup> energy (eV)	2S cross section (10 <sup>-18</sup> cm <sup>2</sup> )	Standard deviation
14.57	0.009	0.015
14.77	0.073	0.016
14.98	0.241	0.013
15.19	0.477	0.020
15.49	0.808	0.021
15.79	1.28	0.025
16.81	2.17	0.047
17.81	2.44	0.041
18.84	2.62	0.037
20.86	2.87	0.041
23.90	2.94	0.046
28.98	3.21	0.050
34.05	3.28	0.052
39.10	3.40	0.053
45.21	3.45	0.049
49.26	3.47	0.059
54.33	3.51	0.051
59.38	3.52	0.062
69.58	3.48	0.070
79.68	3.40	0.069
89.88	3.33	0.062
89.88*	3.35	0.066
99.88	3.24	0.067
99.88*	3.27	0.056
120.28*	3.12	0.053
140.58*	2.95	0.059
160.78*	2.74	0.054
181.28*	2.63	0.048
201.58*	2.45	0.044
252.38*	2.17	0.039
303.18*	1.94	0.032
404.78*	1.63	0.031
506.18*	1.43	0.031

<sup>a</sup>Normalized to the absolute measurements at 39.10 eV.

<sup>b</sup>The asterisked values were taken using an accelerating focus mode of the electron gun. Values without asterisks were taken using the decelerating mode (Ref. 9). Overlap between the two focusing modes was examined at electron energies of 90 and 100 eV.

of Miller and Krauss<sup>36</sup> and the theoretical optical oscillator strengths and transition probabilities of Allison and Dalgarno.<sup>37</sup> From this normalization, the sensitivity of their optical detection system (the same detection system used in the Vroom and de Heer measurements) could be determined for Lyman- $\alpha$  radiation. Using this normalization procedure, de Heer and Carrière showed that the Vroom and de Heer<sup>2</sup> results should be lowered by a factor of 1.31.

The present results using rf quenching do not need a polarization correction (see Appendix). However, it has been found by Ott *et al.*<sup>6</sup> that radiation from 2S hydrogen atoms quenched in a dc electric field is partially polarized because of

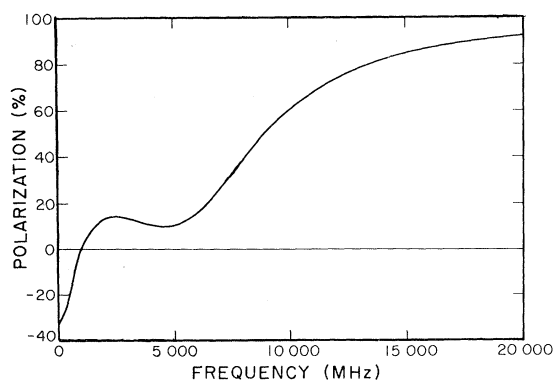


FIG. 12. Polarization, as a function of frequency, of Lyman- $\alpha$  radiation due to rf quenching of metastable hydrogen and deuterium atoms.

mixing of the 2S state with both of the P states. The polarization was found to be about -30%, which would increase the Vroom and de Heer<sup>2</sup> results by 10%. At 400 and 500 eV the Vroom and de Heer<sup>2</sup> results, corrected for polarization and divided by 1.31, are found to agree within experimental error with the present results are shown in Fig. 11.

The shape of the 2S dissociative excitation cross section is different in the two measurements. The value for the cross section as measured by Vroom and de Heer<sup>2</sup> falls off monotonically from the lowest electron energy (50 eV) to the highest (6 keV). The more recent measurements of de Heer and Carrière<sup>35</sup> on Lyman- $\alpha$  from H(2P) after dissociative excitation from H<sub>2</sub> indicate that below 100 eV the cross sections of Vroom and de Heer rise too much towards lower energy. In the present results the cross section peaks between 60 and 70 eV and then does not fall off with energy as rapidly as the Vroom and de Heer<sup>2</sup> results.

A tabulation of the present results for the 2S

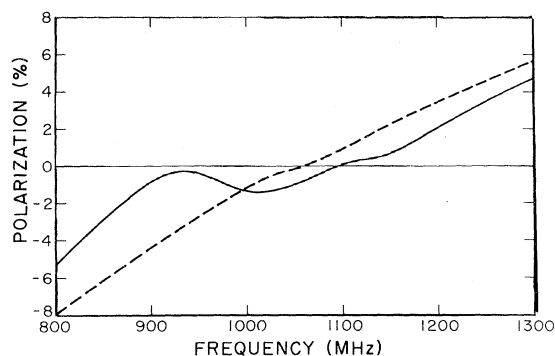


FIG. 13. Polarization as a function of frequency, near the  $^2S_{1/2}$ - $^2P_{1/2}$  resonance, of Lyman- $\alpha$  radiation due to rf quenching of metastable hydrogen atoms (solid line) and the deuterium atoms (broken line).

TABLE IV. Polarization of Lyman- $\alpha$  radiation produced by rf quenching of metastable hydrogen and deuterium atoms.

Frequency (MHz)	P(H)(%)	P(D)(%)
0	-32.31	-32.65
500	-18.81	-19.85
750	-7.60	-9.84
1000	-1.37	-1.18
1025	-1.37	-0.56
1050	-0.99	-0.17
1060	-0.78	0.00
1070	-0.54	+0.20
1080	-0.31	+0.42
1090	-0.08	+0.67
1100	+0.11	+0.93
1250	+3.47	+4.56
1500	+8.45	+8.89
2000	13.17	13.29
4000	10.29	10.20
5000	10.10	9.96
6000	15.90	15.66
7000	26.79	26.47
8000	39.46	39.10
9000	51.21	50.84
10000	60.04	60.39
15000	84.75	84.65
20000	92.18	92.13

dissociative excitation cross section, together with the calculated standard deviation, is given in Table III. To obtain the values listed in Table III the relative results have been normalized to the absolute value of the cross section at 39.1 eV.

#### ACKNOWLEDGMENTS

The authors are indebted to Professor H. Kleinpoppen for suggesting the use of rf quenching in this type of measurement and to Dr. Alan Gallagher for advice in the polarization calculations outlined in the Appendix. We thank Dr. F. J. de Heer and Dr. J. C. Carrière for discussions of their measurements prior to publication. The authors are indebted to the Laboratory for Atmospheric and Space Physics for use of facilities for absolute calibration of the quantum efficiency and gain of the photomultiplier.

#### APPENDIX

The polarization of the radiation emitted when an oscillating electric field quenches metastable 2S atoms has been calculated using the Breit<sup>38</sup> formulation as outlined by Franken.<sup>39</sup>

The system is initially in a set of states  $a$ , undergoing stimulated absorption to an intermediate state  $c$ , followed by spontaneous emission to the final state  $b$ .

The intensity of the emitted radiation can be expressed in the form

$$I^{\sigma,\pi} \propto \sum_{abcc'} f_{ca} f_{ac'} g_{c'b}^{\sigma,\pi} g_{bc}^{\sigma,\pi} \times \left[ \frac{1}{(\omega - \omega_{ca} + \frac{1}{2}i\Gamma)(\omega - \omega_{c'a} - \frac{1}{2}i\Gamma)} + \frac{1}{(-\omega - \omega_{ca} + \frac{1}{2}i\Gamma)(-\omega - \omega_{c'a} - \frac{1}{2}i\Gamma)} \right], \quad (\text{A1})$$

where  $a$  is the initial  $2^2S_{1/2}$  state with quantum numbers  $F$  and  $m$ ,  $b$  is the final  $1^2S_{1/2}$  state with quantum numbers  $F'$  and  $m'$ ,  $c$  is the intermediate  $2^2P_{1/2}$  state with quantum numbers  $J$ ,  $G$ , and  $\mu$ ,  $c'$  is the intermediate  $2^2P_{3/2}$  state with quantum numbers  $J'$ ,  $G'$ , and  $\mu'$ ,  $\omega_{ca} \equiv \omega_{JG\mu, Fm} = \omega_{JG, F}$ ,  $\omega_{c'a} \equiv \omega_{J'G'\mu', Fm} = \omega_{J'G', F}$ ,  $\Gamma$  is the radiative decay constant for the  $2P$  states, and  $\omega$  is the frequency of the applied oscillating electric field.

The  $m_F$  splittings are assumed to be small enough to be ignored with respect to the  $\omega_{JG\mu, Fm}$ .  $\vec{E} = E\hat{z}$  defines the  $\vec{z}$  axis, and  $\vec{E} \cdot \vec{r} = Ez$ .

The  $f$  and  $g$  matrix elements then have the general form

$$f_{cb} \propto \langle {}^2Pc | z | {}^2Sb \rangle, \quad g_{cb}^{\pi} \propto \langle {}^2Pc | z | {}^2Sb \rangle,$$

$$g_{cb}^{\sigma} \propto \langle {}^2Pc | x | {}^2Sb \rangle,$$

where the  $\sigma$  and  $\pi$  refer to the polarization of the  $2P-1S$  radiation. These matrix elements can then be evaluated using the formulas given, for example, in Condon and Shortley.<sup>40</sup>

To put expression (A1) into a more useful form, it is expanded in terms of the  $F$ 's,  $G$ 's,  $\mu$ 's, and  $m$ 's:

$$I^{\sigma,\pi} \propto \sum_{\substack{F, m, F', m' \\ JG\mu, J'G'\mu'}} f_{JG\mu, Fm} f_{Fm, J'G'\mu'} g_{J'G'\mu', F'm'}^{\sigma,\pi} g_{F'm', JG\mu}^{\sigma,\pi} \times \left[ \frac{1}{(\omega - \omega_{JG, F} + \frac{1}{2}i\Gamma)(\omega - \omega_{J'G', F} - \frac{1}{2}i\Gamma)} + \frac{1}{(-\omega - \omega_{JG, F} + \frac{1}{2}i\Gamma)(-\omega - \omega_{J'G', F} - \frac{1}{2}i\Gamma)} \right]. \quad (\text{A2})$$

The two expressions with the  $\omega$ 's in the denominator are seen to be functions of  $JGJ'G'F$  only and can be labeled as

$$S_{JG, J'G'}^F(\omega).$$

Then

$$I^{\sigma, \pi} \propto \sum_{JG, J'G'F} S_{JG, J'G'}^F(\omega) \sum_{\mu\mu'} \left( \sum_m f_{JG\mu, Fm} f_{Fm, J'G'\mu'} \right) \\ \times \left( \sum_{F'm'} g_{J'G'\mu', F'm'}^{\sigma, \pi} g_{F'm', JG\mu}^{\sigma, \pi} \right).$$

Now by defining

$$\sum_{F'm'} g_{J'G'\mu', F'm'}^{\sigma, \pi} g_{F'm', JG\mu}^{\sigma, \pi} = C_{J'G'\mu', JG\mu}^{\sigma, \pi}$$

and

$$\sum_m f_{JG\mu, Fm} f_{Fm, J'G'\mu'} = D_{J'G'\mu', JG\mu}^F,$$

where the superscript  $F$  refers to the 2S hyperfine levels, the final result can be expressed as

$$I^{\sigma, \pi} \propto \sum_{JG, J'G'F} S_{JG, J'G'}^F(\omega) \\ \times \left( \sum_{\mu\mu'} D_{J'G'\mu', JG\mu}^F C_{J'G'\mu', JG\mu}^{\sigma, \pi} \right). \quad (\text{A3})$$

Since  $I_{\perp} \equiv I^{\sigma}$  and  $I_{\parallel} \equiv I^{\pi}$ , the fractional polarization is given by

$$P = (I^{\pi} - I^{\sigma}) / (I^{\pi} + I^{\sigma}). \quad (\text{A4})$$

For hydrogen in the limit of zero frequency (dc electric field) the polarization was found to be  $-32.31\%$ , which is in agreement with the earlier calculations of Casalese and Gerjuoy,<sup>7</sup> who obtained a value of  $-32.33\%$ .

The general shape of the polarization as a function of frequency for both hydrogen and deuterium is shown in Fig. 12. The frequency range extends from 0 to 20 000 MHz. On the scale shown differences between hydrogen and deuterium are small and only one curve is drawn. In the frequency range 800–1300 MHz the differences between the polarization of Lyman- $\alpha$  radiation emitted from H(2S) atoms and that from D(2S) atoms are shown in Fig. 13. The polarization is seen to go to zero at 1060 MHz for deuterium and at 1093 MHz for hydrogen. A few tabulated values are given in Table IV.

\*Work supported by the National Science Foundation under Grant No. GP-17174.

†Present address: Department of Physics, New York University, New York, N. Y. 10003.

‡Staff Member, Laboratory Astrophysics Division, National Bureau of Standards.

<sup>1</sup>W. E. Lamb, Jr. and R. C. Retherford, Phys. Rev. **79**, 549 (1950).

<sup>2</sup>D. A. Vroom and F. J. de Heer, J. Chem. Phys. **50**, 580 (1969).

<sup>3</sup>W. L. Fite and R. T. Brackmann, Phys. Rev. **112**, 1151 (1958).

<sup>4</sup>J. W. McGowan, J. F. Williams, and D. A. Vroom, Chem. Phys. Letters **3**, 614 (1969).

<sup>5</sup>G. H. Dunn, Phys. Rev. Letters **8**, 62 (1962).

<sup>6</sup>W. R. Ott, W. E. Kauppila, and W. L. Fite, Phys. Rev. A **1**, 1089 (1970).

<sup>7</sup>J. S. Casalese and E. Gerjuoy, Phys. Rev. **180**, 327 (1969).

<sup>8</sup>H. A. Bethe and E. E. Salpeter, *Quantum Mechanics of One and Two Electron Systems* (Academic, New York, 1957).

<sup>9</sup>R. L. Long, D. M. Cox, and S. J. Smith, J. Res. Natl. Bur. Std. **72A**, 521 (1968).

<sup>10</sup>G. E. Chamberlain, S. J. Smith, and D. W. O. Heddle, Phys. Rev. Letters **12**, 647 (1964).

<sup>11</sup>K. Watanabe, Advan. Geophys. **5**, 153 (1958).

<sup>12</sup>K. Watanabe, F. M. Matsunaga, and H. Sakai, Appl. Opt. **6**, 391 (1967).

<sup>13</sup>M. Leventhal, R. T. Robiscoe, and K. R. Lea, Phys. Rev. **158**, 49 (1967).

<sup>14</sup>M. Misakian and J. C. Zorn, Phys. Rev. Letters **27**, 174 (1971); M. Misakian, thesis (University of Michigan, 1971) (unpublished).

<sup>15</sup>P. N. Stanton and R. M. St. John, J. Opt. Soc. Am. **59**, 252 (1969).

<sup>16</sup>Type GM 110 McLeod gauge, manufactured by Consolidated Vacuum Corporation.

<sup>17</sup>K. Nakayama, Y. Akiyama, and H. Hasimoto, Vacuum

**18**, 2 (1968).

<sup>18</sup>A. W. Porter, Trans. Faraday Soc. **29**, 702 (1933).

<sup>19</sup>P. Rosenberg, Rev. Sci. Instr. **9**, 258 (1938); **10**, 131 (1939).

<sup>20</sup>O. Klemperer, J. Sci. Instr. **21**, 88 (1944).

<sup>21</sup>W. Gaede, Ann. Physik **46**, 354 (1915).

<sup>22</sup>H. Ishii and K. Nakayama, *Transactions of the Eighth National Vacuum Symposium* (Pergamon, New York, 1961), p. 519.

<sup>23</sup>C. Meinke and G. Reich, Vacuum **13**, 579 (1963).

<sup>24</sup>R. J. Tunnicliffe and J. A. Rees, Vacuum **17**, 457 (1967).

<sup>25</sup>M. Rusch and O. Bunge, Z. Tech. Physik **13**, 77 (1932).

<sup>26</sup>H. H. Podgurski and F. N. Davis, J. Phys. Chem. **65**, 1343 (1961).

<sup>27</sup>T. Edmonds and J. P. Hobson, J. Vacuum Sci. Tech. **2**, 182 (1965).

<sup>28</sup>C. G. J. Jansen and A. Venema, Vacuum **9**, 219 (1959).

<sup>29</sup>P. H. Carr, Vacuum **14**, 37 (1964).

<sup>30</sup>B. Bederson and W. L. Fite, *Methods of Experimental Physics* (Academic, New York, 1968), Vol. 7A.

<sup>31</sup>Calibration was done by Standards Laboratory, Ball Brothers Research Corporation, Boulder, Colo.

<sup>32</sup>M. C. Johnson, Appl. Opt. **7**, 879 (1968).

<sup>33</sup>D. Rapp, T. E. Sharp, and D. D. Briglia, Phys. Rev. Letters **14**, 533 (1965).

<sup>34</sup>J. C. Carrière and F. J. de Heer, J. Chem. Phys. (to be published).

<sup>35</sup>F. J. de Heer and J. C. Carrière, J. Chem. Phys. (to be published).

<sup>36</sup>K. J. Miller and M. Krauss, J. Chem. Phys. **47**, 3754 (1967).

<sup>37</sup>A. C. Allison and A. Dalgarno, At. Data **1**, 289 (1970).

<sup>38</sup>G. Briet, Rev. Mod. Phys. **5**, 91 (1933).

<sup>39</sup>P. A. Franken, Phys. Rev. **121**, 508 (1961).

<sup>40</sup>E. U. Condon and G. H. Shortley, *The Theory of Atomic Spectra* (Cambridge U.P., New York, 1964).